energies

MDPI

Article

Electromagnetic Shielding Effect of a Canned Permanent Magnet Motor

Kun Hu [1], Haijun Zhuang [1,*] and Qiang Yu [2]

[1] School of Electrical and Power Engineering, China University of Mining and Technology, Xuzhou 221116, China; hucaipan@126.com

[2] School of Information and Control Engineering, China University of Mining and Technology, Xuzhou 221116, China; yuqiang@cumt.edu.cn

* Correspondence: ts18130090a31@cumt.edu.cn; Tel.: +86-157-0527-8075

Received: 11 July 2020; Accepted: 4 September 2020; Published: 8 September 2020

Abstract: Due to use of the metallic cans in the air gap, the electromagnetic shielding effect is formed, which is the prominent characteristic of the canned motor. In the flux field, eddy current induction occurs on both cans that thus affects the characteristic of the air gap flux field, and generates a loss that is the highest loss of the canned motor. In this paper, a combination method is proposed and stressed to analyze the shielding effect, based on a typical canned permanent magnet synchronous motor. First, the *dq* vector decomposition of the eddy current is studied. Second, the effect of the load angle on the loss distribution is studied. Finally, compared with the ordinary motor, the feature of can loss due to rotor speed and conductivity variation is shown. The three-dimensional finite element method is adopted, considering the end effect.

Keywords: canned electrical motor; can loss; shielding effect; eddy current; permanent magnet motor

1. Introduction

The canned machine is usually applied in the chemical and nuclear field as a pump drive, to convey poisonous and high pressure liquid [1,2]. Poisonous, corrosive and high pressure liquid may get into the air gap, thus two metallic cans are respectively fixed in the air gap, which can prevent the leakage of transportable liquid. In this harsh working environment, high reliability ensures the shielding motor operates normally for a long time.

Electromagnetic shielding phenomenon is formed, this is due to the cans that are used in the air gap. The can is made up of the bulk metal instead of lamination, which is limited by the manufacturing craft. The shielding material is nonmagnetic and has low conductivity to suppress the eddy current, such as a nickel based alloy. In an alternating flux field, an eddy current induction occurs on the cans and generates a loss that is called can loss here. Meanwhile, the eddy induction also forms a flux field that affects the original one in return, as well as affects distinctly the output performance of the motors.

A traditional canned motor is mainly the squirrel cage induction motor [3–6]. However, the induction cage structure may break due to a higher temperature rise of rotor that is caused by can loss. In [7], the number of stator slots is further increased to 48 and the double-layer armature coil structure is adopted to make the air gap magnetic field more sinusoidal, thereby reducing can loss. However, in the pumping industry, with increasing demand of high efficiency, reliability and control flexibility, canned permanent magnet motors are a good solution [8,9]. A high temperature rise of the rotor leads to interior permanent magnet synchronous motors demagnetizing, due to the poor cooling environment of the shielding motors, and thus the interior permanent magnet synchronous motors are not suitable for the shielding motor. The surface mounted PMs topology is investigated, which can be effective to avoid demagnetizing caused by excessive working temperature.

Fractional slot tooth concentrated windings (FSCW) have stimulated research interest [10,11]. This winding configuration shows shorter end winding, the higher fault tolerance rate, the lower manufacturing cost, the harder mechanical characteristics, and higher efficiency. Meanwhile, the windings have no overlap between each other, so the interphase insulation is well. However, in terms of the magneto motive force (MMF) contents, the air gap magnetic field of the permanent magnet synchronous motor is not sinusoidal, resulting in certain harmonics. Apart from the working harmonic that generates electromagnetic torque, the odd harmonics cause a lot of problems as vibration, noise and heat [12–14]. A canned permanent magnet synchronous motor with FSCW is studied, with emphasis placed on can loss and the air gap flux field.

The electromagnetic shielding analysis is emphasized in the canned motor theoretical analysis. In [15], the mechanism and characteristics of the eddy current induction and the loss of the DC canned motor under different excitation are studied. The main research methods of conventional motors include finite element (FE) [16–19], the analytical method [20] and empirical formulas [21–23]. The empirical formulas method uses arithmetic expression to estimate the loss as the corresponding function, which can quickly and roughly calculate the average value of the can loss. In [24], the can loss is calculated by a multilayer analytical model. However, traditional analysis methods cannot directly be applied to canned motors, the eddy current and the can loss distribution in space, and the *dq* vector decomposition of the eddy current is not well studied. In this paper, a canned permanent magnet synchronous motor is studied. The organization of the paper is as follows. In Section 2, the studied canned PM motor is described. In Section 3, the calculation method is introduced and the *dq* vector decomposition of eddy induction and can loss is discussed. In Section 4, the influence of the load angle on eddy induction and can loss distribution is analyzed. In Section 5, can loss and flux harmonics due to rotor speed and load is studied.

2. The Canned PM Motor

In Figure 1 a 2D sketch of the stator and rotor is shown, with an appropriate choice of the slot-pole that helps reduce copper consumption and loss. The motor is featured with concentrated coil, this typology exhibits: (1) a lower cogging effect and torque ripple, which are beneficial for the shielding motor to adjust the fluid at a low speed; (2) the higher fault tolerance rate, the lower production cost and the harder mechanical characteristics; (3) good manufacturability, simple off-line and higher copper space factor and (4) good interphase insulation. The motor adopts the stator split ratio design, which has stronger air gap flux density and lower yoke flux saturation.

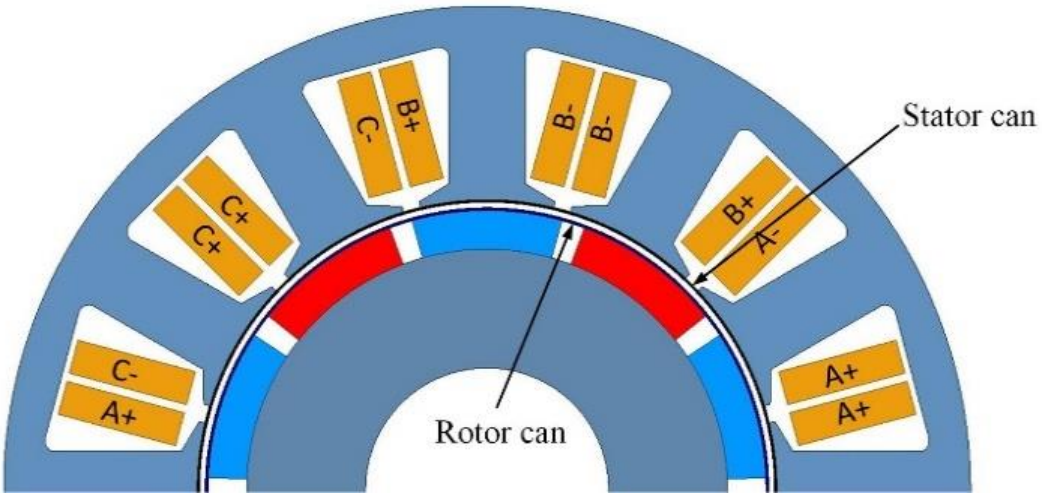

Figure 1. 2D sketch of the canned PM motor.

The major dimensional parameters are listed in Table 1. A couple of cans were fixed in the air gap, namely the stator can and rotor can. The rotor can was fixed onto the bore of the rotor part to protect the PMs from corrosion, meanwhile the stator can was fixed onto the inner surface of the stator teeth to protect the armature winding. To accommodate the cans and PMs, the air gap width with magnets reached to 9 mm. Due to the width of the air gap being artificially increased to install the cans, the mutual inductance could be ignored. To resist the centrifugal force, the radial width of cans reached up to 0.5 mm, which could be correspondingly increased for larger canned motors. The can material was Hastelloy C, a nickel-based nonmagnetic alloy with low electrical conductivity that restrains the eddy current. The value was 800,000 S/m at 20 °C and approximately 1.4 times lower at every 100 °C rise. For the conductivity of both cans, the value at the steady-state temperature was preset. Due to that, the temperature rise on the can only affected the intensity of the eddy current and loss, but did not affect the characteristics of its distribution on cans, thus a conductivity change that was caused by the temperature rise was not considered in this paper. Note that the air gap flux field change was caused by the eddy current, and not by the magnetoresistance change that was caused by the material.

Table 1. The main canned machine's geometrical parameters.

Rated Power (kW)	**6.5**	**Rotor Can Thickness (mm)**	**0.5**
Rated Voltage (V)	**380**		
Can alloy	Hastelloy C	Stator can thickness (mm)	0.5
Axial length (mm)	67	Rated speed (rpm)	1700
Air gap width with magnets (mm)	9	Magnet material	NdFe35
Stator outer bore diameter (mm)	175	Magnet thickness (mm)	7
Number of turns per phase	136	Stator/rotor material	DW465-50
Connection of winding	Wye	Number of strands	18
Q-axis current amplitude (A)	43.3	D-axis current amplitude (A)	25

3. Field Distribution Analysis Method

For the can, the corresponding conductivity is given. To illustrate the mechanism of can loss, the multilayer analytical model was introduced. The motor can be regarded as a multilayer model with the corresponding boundary conditions between each layer, as to constitute the boundary conditions of Maxwell's equations. The can loss was obtained by calculating the electromagnetic energy flow based on Poynting's vector. The energy vector is defined as $\vec{S} = \vec{E} \times \vec{H}$, H and is the magnetic field intensity and E is the electrical field density.

For the sinusoidal time-varying electromagnetic fields, the active power was the average power p_{ave}. The energy vector caused by each harmonic was summed up, and thus can loss could be calculated by integrating the surface Ω of both cans layer, which can be written as

$$P_{ave} = -\frac{1}{2} \iint_{\Omega} Re\left\{\vec{E} \times \vec{H}^{*}\right\}^{r} n d\Omega \quad (1)$$

where n is the unit vector vertical to Ω and the r is the radius of each part of the motor components. When conducting detailed theoretical deduction, the mathematical model of can loss and conductivity is the linear model.

The eddy current and loss were calculated with FE by Maxwell in this paper. This method discretizes the solution region into many small subregions, applying the principle of solving the boundary problem to these subregions, and then the results of each subregion are summed up to get the solution of the whole region. For the FE model, all the motor segments were columnar and separated from each other. The cylinder was meshed to make the solution domain more circular and thus improve the calculation accuracy. Too many grids consumed too much of the solution time, so each cylinder was polygonized up to 180 sectors.

In this paper, using the direction method we calculated can loss, based on each mesh element i with flux density $B_i(t)$. Loss density P_i can be seen as a function of the square rate of change of $B_i(t)$, which is

$$P_i = \frac{1}{T}\int_0^T \frac{a}{2\pi^2}\left(\frac{dB_i(t)}{dt}\right)^2 dt \tag{2}$$

where the Steinmetz coefficient is represented by a and T means the time period. By discretizing Equation (2), we get

$$P_i = \frac{a}{2\pi^2}\cdot\frac{1}{T\cdot\Delta t}\sum_{i=1}^{N}\left(B_{i\_k+1} - B_{i\_k}\right)^2 \tag{3}$$

where Δt is the time of two discretized units in a subregion and n is the number of steps during T. Then the can loss is written as

$$P = \sum_{i=1}^{M} m_i P_i = \frac{a}{2\pi^2}\cdot Nf^2\sum_{i=1}^{M}\left[m_i\sum_{i=1}^{n}\left(B_{i\_k+1} - B_{i\_k}\right)^2\right] \tag{4}$$

where m_i is the mass of i-th element, M is the total number of subregion and f is the frequency.

A flux path with and without cans is shown in Figure 2. The ideal 3-phase sinusoidal AC excitation with a rated load was applied. Through the stator teeth, yoke, air gap, PMs and rotor yoke, the main flux loop was formed and was similar in both motors. Due to the use of cans in the air gap that led to the eddy current induction and thus the magnetic energy consumption in the stator and rotor parts, the flux density was slightly reduced.

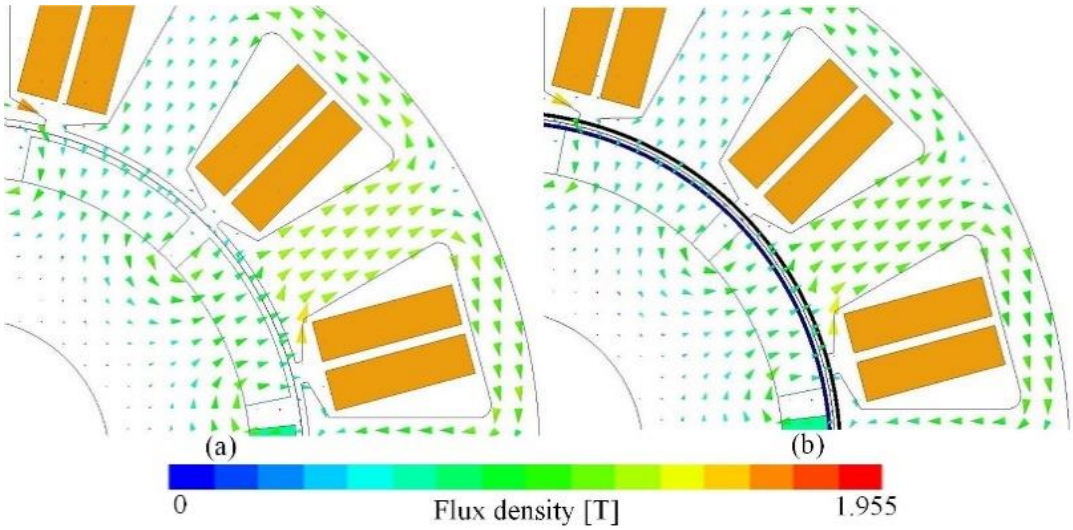

Figure 2. Comparison of the flux patch due to the use of cans: (**a**) the ordinary motor and (**b**) the canned motor.

The eddy current and can loss on both cans were spatial and temporal distribution. An ideal working current could be decomposed into the dq axis current. As to both cans, the eddy current and can loss induced by different currents are shown, and the vector relationship of the eddy current and can loss between different currents was analyzed. Note that the same color code has different amplitudes in the figures below, in order to better show the distribution of the current and loss on both cans.

3.1. Eddy Current Due to the d Axis Current

Injecting only the *d* axis current, the eddy current and loss on cans are respectively shown in Figure 3. As to the stator can, Figure 3a,b shows eddy current induction, which had the following characteristics: (1) in general, a 10-swirl induction from the armature coil, and the neighboring ones were of alternative rotation, namely clockwise and counterclockwise; (2) for a single swirl, the layout structure with a couple of main channels that went along the axial span, as well as their connecting bridges respectively at the lower and upper side is shown and (3) for the couple of channels in a swirl, the opposite direction stemmed from the alternative magnetization directions of armature coils. The eddy current on the stator can was concentrated in channels and bridges. The main reasons are: (1) for the connection areas of neighboring swirls, the current density was either intensified or offset, depending on the revolution direction of each swirl, namely the channel effect here and (2) as the flow path of the eddy current became narrowed, which caused the eddy current density to increase, the end effect due to the use of cans was formed. Consequently, Figure 3d shows the ohmic loss distribution. Likewise, the swirl-like generation demonstrated the intensification areas at bridges and some of the channels where swirls were intensified.

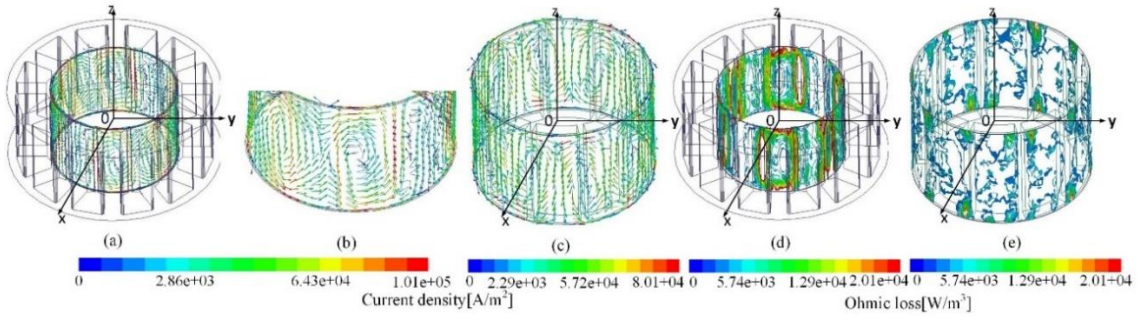

Figure 3. Eddy induction and loss distribution on cans due to the *d* axis current, (**a**) eddy current on the stator can, (**b**) local detail on the stator can, (**c**) eddy current on the rotor can, (**d**) loss on the stator can and (**e**) loss on the rotor can.

As to the rotor can, Figure 3c–e respectively shows the eddy current and loss distribution. Similar eddy induction occurred, however the density was comparatively much lower. This is due to the synchronous rotation of the rotor can that disables the cut by the air gap flux field. However, swirls still exist, due to the cogging effect that made a slight relative motion between the air gap field and the rotating can. Consequently, the loss was considerably lower, even if the end effect looked moderate.

3.2. Eddy Current Due to the q Axis Current

Figure 4 shows the eddy current and loss distribution on cans when alternatively the *q* axis current was injected. As to the stator can, Figure 4a,b shows the eddy current. Compared to Figure 3, a similar swirl-like distribution was demonstrated. However, difference points are listed as follows: (1) higher density; (2) deviation of all excited channels that was originally parallel to the Z-axis and (3) an angular shift of 90° in an electrical degree for the excited 10-swirl configuration, based on the Z-axis, compared to Figure 3a. The reasons are as follows. As to (1), the amplitude of the *q* axis current was greater. As to (2), the angular positional shift of the rotation part led to the redirection of the air gap flux, and thus to the shift of the excited swirls. As to (3) the *dq* axis current differs by 90° in an electrical angle in the terms of time.

As to the rotor can, Figure 4c shows the eddy current. Likewise, a similar distribution and a higher density due to greater amplitude of the *q* axis current are demonstrated.

Consequently, Figure 4d,e shows the can loss on both cans, with a swirl-like distribution in the analogy. Accordingly, the intensification areas at channels or bridges occurred due to the channel

effect as well as the end effect. Note that the density on both cans was comparatively higher, due to higher eddy induction density.

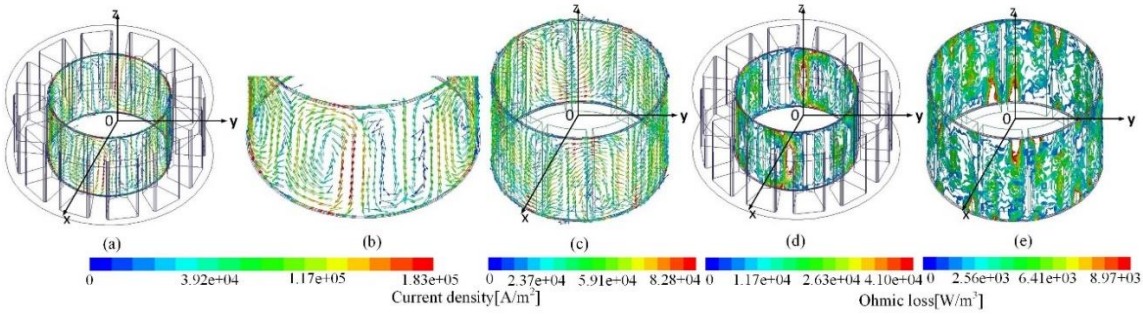

Figure 4. Eddy current and loss distribution on cans due to the *q* axis current, (**a**) eddy current on the stator can, (**b**) local detail, (**c**) eddy current on the rotor can, (**d**) loss on the stator can and (**e**) loss on the rotor can.

3.3. Eddy Current Due to the Working Current

Finally, the eddy current and loss distribution due to the use of cans were obtained by the combination of the regarded field respectively by *dq* excitations. Such a method was realized by the combination of space vectors for each regarded magnetic field. Accordingly, the eddy current and can loss are shown in Figure 5, which had the following characteristics: (1) the eddy current and loss distribution on both cans was basically consistent with that under the action of the *q* axis current; (2) the density of channels and bridges was less than that under the action of the *q* axis current and (3) the degree of channel deviation was less than that induced under the *q* axis current.

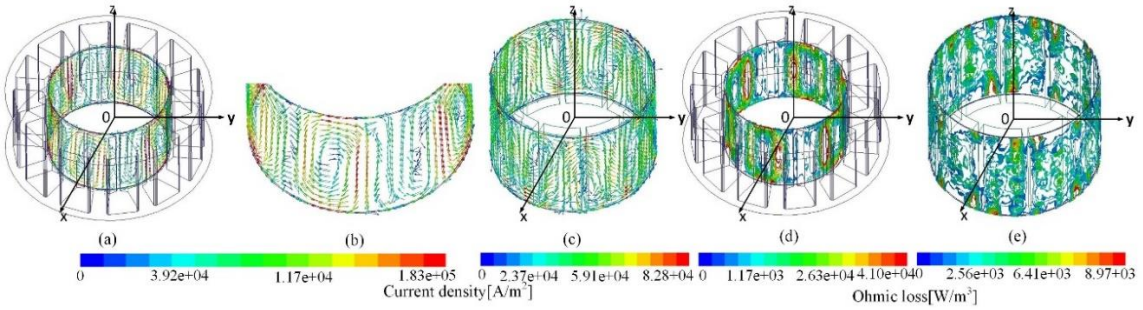

Figure 5. Eddy current and loss distribution on cans due to the working current, (**a**) eddy current on the stator can, (**b**) local details, (**c**) eddy current on the rotor can, (**d**) loss on the stator can and (**e**) loss on the rotor can.

The above figures show the eddy current generated by different excitations, the vector relationship among them is discussed below. Due to the current angle, the relative position of the flux field that formed by *dq* current was different. At the rated current angle of 30°, the *dq* current was decomposed, and thus the amplitude of the *q* axis current was higher than that of the *d* axis current that led to the density of the eddy current and the loss was higher under the *q* axis current. For the vector superposition of eddy induction on the stator can, although the eddy current distribution under the *dq* current differed by 90° in electrical degree, the density of the eddy current induced by the *q* axis current was higher than that induced by the *d* axis current, so the superposed eddy current distribution still exhibited the *q* axis eddy current distribution, the density of the superposed eddy current was less than that induced by the *q* axis eddy current and weakened the deviation of all excited channels. Due to the synchronous speed of the rotor can, eddy current vector superposition still exhibited the eddy current distribution under the action of the *dq* current. In short, the distribution of the eddy current induced by the working current could be decomposed into that induced by the *dq* axis current.

4. Influence of the Load Angle Change on the Eddy Current and Loss Distribution

Different load angles led to the density and spatial distribution change of the flux field at the same time, as well as resulted in current and loss distribution change on the both cans. The flux and loss at a load angle of 30° are shown in Figure 6. Figure 6a,b respectively demonstrates the spatial flux field at a load angle of 60° and 30°, the difference lies in that: (1) the flux density was higher at the greater load angle of 60°, as the higher flux density was required and (2) the main flux did not vertically pass through the air gap, i.e., the air gap flux path that connects a stator pole and magnet, and deviated with an increasing load angle.

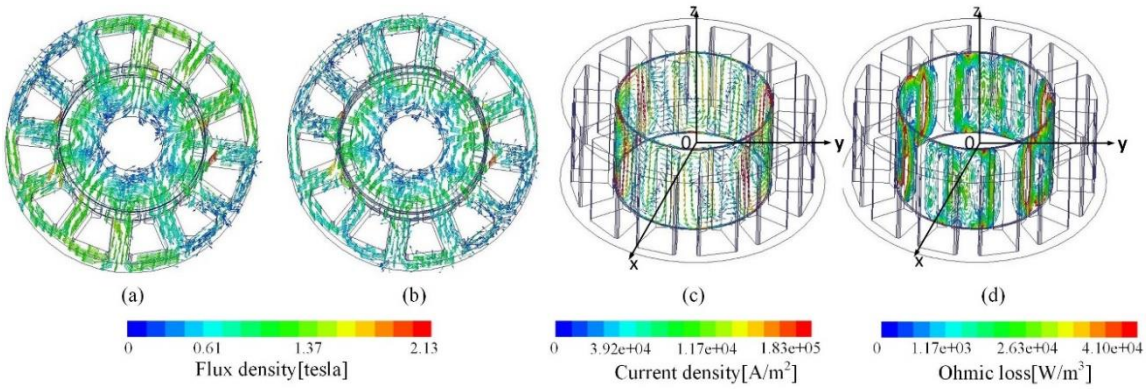

Figure 6. Flux and loss distribution due to different load angles, (**a**) flux density at 60°, (**b**) flux density at 30°, (**c**) eddy current on the stator can and (**d**) loss on the stator can.

Consequently, comparing with Figure 5a–d, the eddy current and loss on the stator can at a load angle of 30° had the following characteristics: (1) as to the eddy induction, the density of swirls was lower, due to lower flux density; (2) for a single swirl, the deviation of channel was lower, due to lower main flux path deviation; (3) as to loss, a swirl-like distribution and lower density occurred, due to a low source of eddy current and (4) as to spatial distribution, the eddy current and loss position had angular shifts of relatively 30° in the electrical angle. Likewise, as to the rotor can, a similar swirl-like distribution and a lower density occurred.

5. Loss and Harmonic Analysis

5.1. Analysis of Air Gap Flux Harmonics

The metallic shielding cans were fixed in the air gap, the feature of flux was changed due to the eddy current. Consequently, Figure 7 respectively shows the flux density harmonics of two motors that is the standard and canned at no and rated load. It is demonstrated that: (1) as to the overview, the 5th harmonic was the working harmonic, the 15th harmonic was the dominant harmful harmonic that distorted the air gap flux field and the 7th harmonic and 17th harmonic increased at the same time; (2) as to the load effect, the amplitude of harmonics increased, due to the greater air gap flux density and (3) as to the shielding effect, the amplitude of harmonics was slightly reduced. This is due to the energy of some harmonics being converted into loss on both cans.

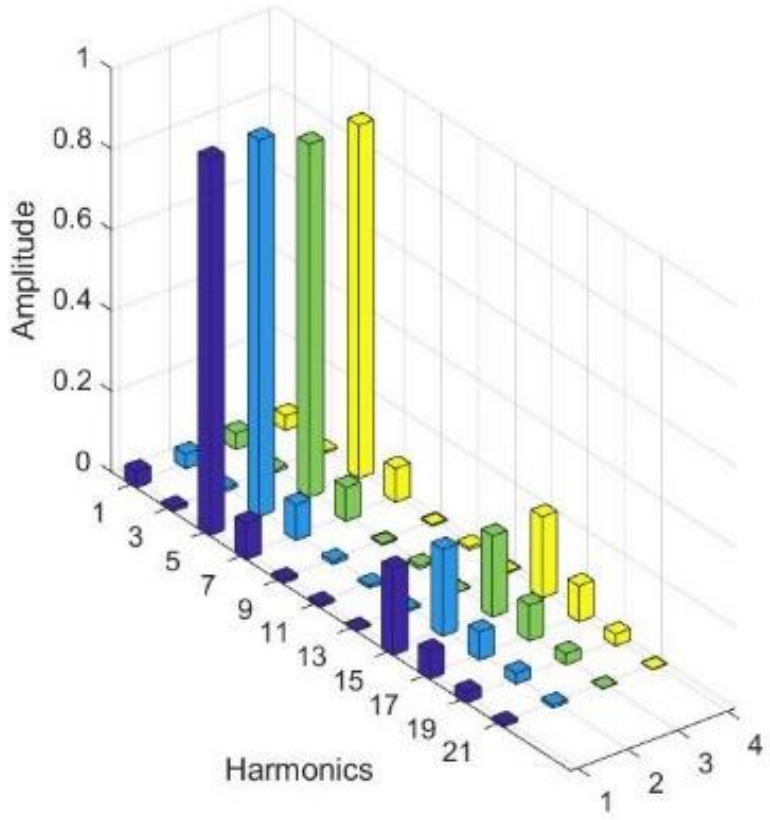

Figure 7. Air gap flux density harmonics due to cans and load. 1 = load without cans, 2 = load with cans, 3 = no load without cans and 4 = no load with cans.

5.2. Can Loss Due to Loads

Table 2 demonstrates can loss that was generated at no and rated loads with rotor speed. The load angle was assigned to 0, that is, the current angle was assigned to 90°, as the no load that facilitated comparison with the rated load. In each case, the loss of both cans increased with speed. For the stator can, the loss increased sharply with speed. When the load was applied, the loss amplitude was approximately 1.2–1.3 times higher under the rated speed. This is mainly due to the higher eddy current caused by intensified flux. As to the rotor can, the loss can be neglected due to the synchronous motion. Consequently, when load was applied, a similar loss density occurred.

Table 2. Can loss (W) with rotor speed.

Speed (krpm)	No Load		Rated Load	
	Stator Can	Rotor Can	Stator Can	Rotor Can
0.2	4.24	0.39	10.88	0.41
0.5	26.32	2.41	30.11	2.48
0.8	66.76	5.91	76.42	6.12
1.1	124.82	10.64	142.94	11.09
1.4	199.34	16.31	228.34	17.07
1.7	259.03	22.58	331.12	23.73

5.3. Can Loss Due to Conductivity

Different materials of shielding can have different conductivity, and conductivity variation affects can loss. Figure 8 shows the shielding loss change with the conductivity variation, which had the following characteristics: (1) in general, the loss increased linearly with conductivity variation, stator can loss was higher than rotor can loss; (2) for the stator can, the shielding loss at the rated

load was higher than that at no load, and the difference between them increased with conductivity variation and (3) as to the rotor can, similar loss characteristics and a lower density occurred, due to the synchronous motion. Low conductivity can be more effective to suppress the eddy current. The canned motors inherence had high operating temperature, which caused conductivity of the can to increase, which reduced the eddy current suppression ability and thus exacerbated the temperature rise of the motor. As to the shielding material, a lower conductivity material is desired.

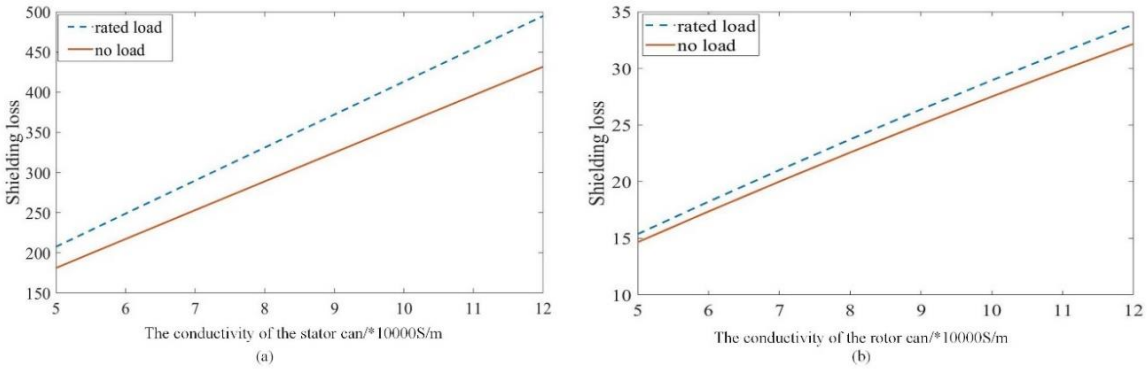

Figure 8. The loss of shielding loss with conductivity variation. (**a**) the conductivity of the stator can, (**b**) the conductivity of the rotor can.

5.4. Experimental Validation

Two permanent magnet synchronous motors that shown in Figure 9 were the objects of this test, one of which was a conventional motor and the other was a shielded motor. In a test bench, a pair of permanent magnet motors with the same geometry was used, but one of them was the shielding motor. The loss of the standard motor included copper loss, iron loss, fiction loss and stray loss, which was applied to obtain iron loss and stray loss. For both motors, the iron loss and stray loss could be seen as the same. The procedure of the test followed these steps. First, using the energy conversion principle to calculate the total loss of the shielding motor. Second, using the sliding test to separate the friction loss. Then, calculating the copper loss by I^2U. Following the above steps, the iron loss and stray loss of the conventional motor were obtained. Finally, the can loss was separated by subtracting the copper loss, iron loss, fiction loss and stray loss from the total loss of the canned motor. Table 3 shows the loss and efficiency that were measured at the rated load and steady state by the test and Table 4 illustrates the loss and efficiency that were measured at no load and the steady state by the test.

Table 3. The loss and efficiency at the rated load. S = standard, C = Canned and * = Estimated.

Sped	Fric (W)		Cop (W)		Ir (W)	Can (W)	Eff (%)
krpm	C	S	C	S	C/S	C	C
0.5	4	1 *	136	134	8	33	85.54
0.8	7	2 *	140	137	15	83	88.87
1.4	10	3 *	147	141	31	246	81.87
1.7	19	5	153	148	47	369	76.92

Table 4. The loss and efficiency at no load. S = standard, C = Canned and * = Estimated.

Sped	Fric (W)		Cop (W)		Ir (W)	Can (W)	Eff (%)
krpm	C	S	C	S	C/S	C	C
0.5	4	1 *	11	10	4	29	-
0.8	7	2 *	14	13	6	72	-
1.4	10	3 *	20	18	13	215	-
1.7	19	5	23	21	17	312	-

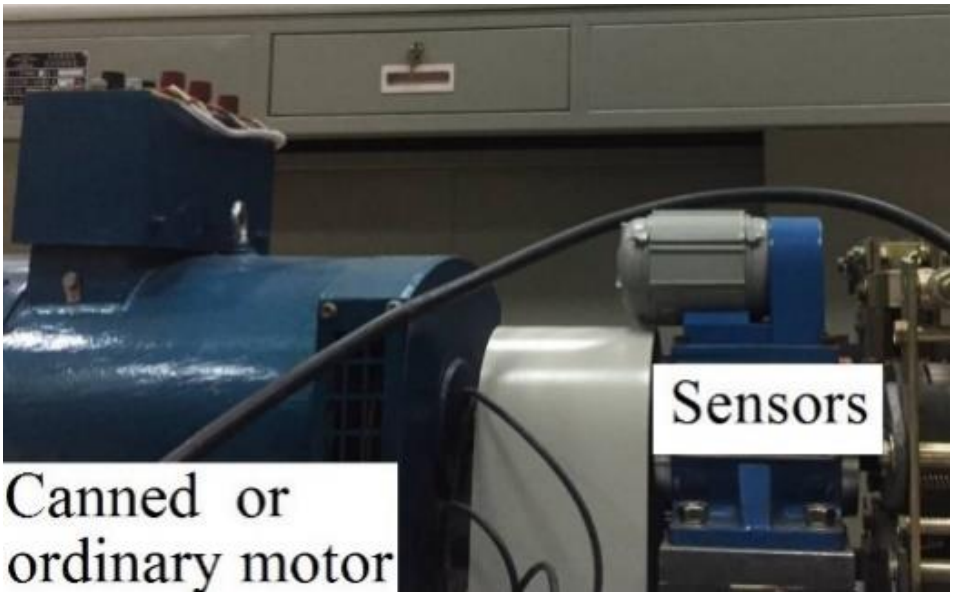

Figure 9. Experimental set up.

The comparison of FE and the measurement due to the use of cans is demonstrated in Figure 10. The tested motor operated in no and rated load, the shielding loss measured by the test was basically the same as that by the FE, the difference between the two ways increased with increasing speed. At no load, the value of the measurement was relatively low, this is due to the overheating that increased the local resistivity of the can at the end, which helped to suppress induced eddy current, but it was not included in 3d. At the rated load, the value of the measurement was higher at lower speeds due to the additional losses caused by the electrical supply harmonics. However, as the speed increased, due to the local resistivity effects, the measured value even fell below 3d. Due to the end effect, the shielding loss measured by 3d was higher than that measured by 2d and the numerical gap was enlarged with the rotor speed.

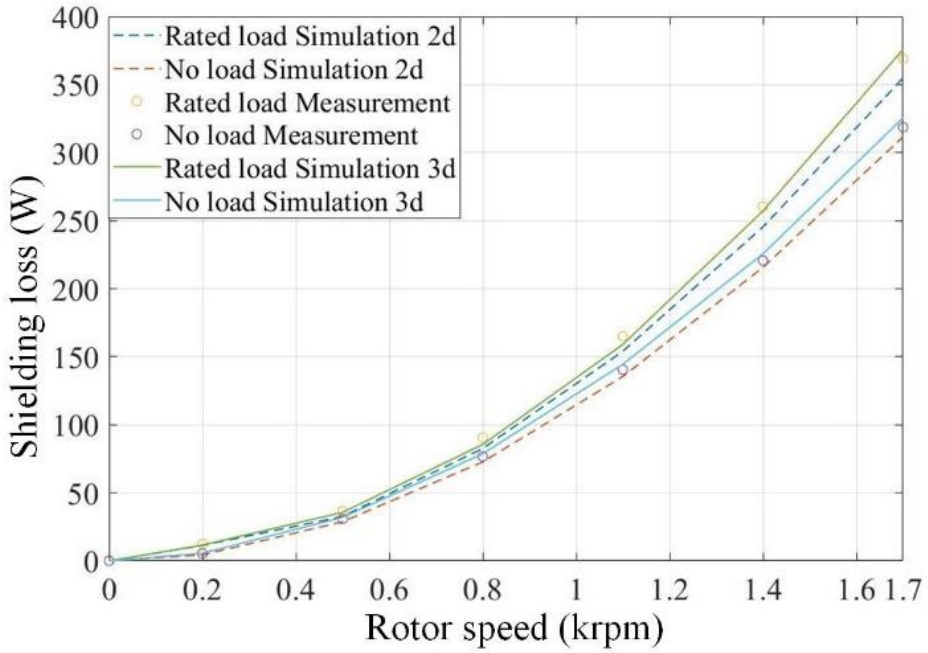

Figure 10. Comparison of finite element (FE) and the measurement due to the cans.

6. Conclusions

For the hydraulic pumps, the canned PM motor was an excellent solution due to the use of metallic cans in the air gap and eddy current induction affecting the performance of the canned motor. In this paper, a canned PM motor with fractional slot tooth concentrated windings was studied. The combination analysis method that clearly shows the eddy current and loss on both cans was proposed. For eddy induction on both cans, it, induced by the working current, can be decomposed into that respectively induced by the *d*–*q* axis current, having the following characteristics: (1) as an overview, the swirl-like eddy current distribution on each can was shown; (2) for a single swirl, the layout structure with a couple of bridges and channels occurred; (3) for the interrelation of swirls, overlap at the channels led to being either positive or negative due to the channel effect and (4) for the end effect due to the use of cans, it made a higher bridges loss. For different loads, the eddy current and loss had similar characteristics of distribution, which had angular shifts by a certain degree in space, and the deviation of the channel changed with the load.

Flux density and loss are further discussed due to the use of cans, the characteristics were as follows: (1) For air gap flux harmonics, the use of cans reduced the 5th working harmonic and suppressed the 15th harmful harmonic. Likewise, the amplitude of harmonics increased with load; (2) For the performance of the can loss, both of the cans loss increased with speed. The stator can loss increased sharply, and the rotor loss could be relatively neglected; (3) For the conductivity of both cans, both losses increased with conductivity variation. Likewise, there was higher loss density at the rated load and negligible rotor can loss. In short, eddy current induced on cans led to an air gap flux field change and loss was generated, changing the output characteristics. An electromagnetic analysis of a canned motor is beneficial to study the control strategy that minimizes losses on both cans.

Author Contributions: Conceptualization, Q.Y.; Methodology, H.Z.; Software, H.Z.; Validation, H.Z.; Formal Analysis, H.Z.; Investigation, H.Z.; Resources, K.H.; Data Curation, H.Z.; Writing-Original Draft Preparation, H.Z.; Writing-Review & Editing, H.Z.; Visualization, K.H.; Supervision, Q.Y., K.H.; Project Administration, K.H.; Funding Acquisition, K.H. All authors have read and agreed to the published version of the manuscript.

Funding: This research received no external funding.

Conflicts of Interest: The authors declare no conflict of interest.

References

1. Robinson, R.C.; Howe, I. The calculation of can losses in canned motors. *Trans. Am. Inst. Electr. Eng.* **1957**, *76*, 312–315.
2. Ergene, L.T. One-slot ac steady-state model of a canned solid rotor induction motor. *IEEE Trans. Magn.* **2004**, *40*, 1892–1896. [CrossRef]
3. Sun, S.L.; Li, J.M. Calculation of electric losses on the shield for canned inductive motor and the ways of its reduction *Large Electr. Mach. Hydraul. Turbine* **1987**, *6*, 30–33.
4. Liang, Y.; Hu, Y.; Liu, X.; Li, C. Calculation and analysis of can losses of canned induction motor. *IEEE Trans. Ind. Electr.* **2014**, *61*, 4531–4538. [CrossRef]
5. Gao, L.; Wei, J.; Li, C.; Liang, Y. Analyses on performances of megawatt double-canned induction motors with different can materials. *IEEE Trans. Energy Convers.* **2017**, *32*, 667–674. [CrossRef]
6. Yu, Q.; Wang, X.; Cheng, Y. Electromagnetic modeling and analysis of can effect of a canned induction electrical machine. *IEEE Trans. Energy Convers.* **2016**, *31*, 1471–1478. [CrossRef]
7. Liang, Y.P.; Bian, X.; Yu, H.B.; Li, C.X. Finite element evaluation and eddy current loss decrease in stator end metallic parts of a large double canned induction motor. *IEEE Trans. Ind. Electr.* **2015**, *62*, 6779–6786. [CrossRef]
8. Yu, Q.; Wang, X.; Cheng, Y. Electromagnetic calculation and characteristic analysis of can effect of a canned permanent magnet motor. *IEEE Trans. Magn.* **2016**, *52*, 1–6. [CrossRef]
9. Burkhardt, Y.; Huth, G.; Urschel, S. Eddy current losses in pm canned motors. In Proceedings of the International Conference on Electrical Machines ICEM 2012, Nicosia, Cyprus, 26–29 September 2012.

10. Wang, J.; Atallah, K.; Zhu, Z.Q.; Howe, D. Modular 3-phase PM brushless machines for in-wheel applications. *IEEE Trans. Veh. Technol.* **2008**, *57*, 2714–2720. [CrossRef]
11. Li, J.; Choi, D.W.; Son, D.H.; Cho, Y.H. Effects of MMF harmonics on rotor eddy current losses for inner rotor fractional slot axial flux permanent magnet synchronous machines. *IEEE Trans. Magn.* **2012**, *48*, 839–842. [CrossRef]
12. Nakano, M.; Kometani, H. A study on eddy-current losses in rotors of surface permanent magnet synchronous machines. *IEEE Trans. Ind. Appl.* **2006**, *42*, 429–435. [CrossRef]
13. Dajaku, G.; Gerling, D. Eddy current loss minimization in rotor magnets of PM machines using high-efficiency 12-teeth-10-slots winding topology. In Proceedings of the International Conference Electrical Machines & Systems, ICEMS 2011, Beijing, China, 20–23 August 2011.
14. Koo, M.; Choi, J.; Hong, K.; Lee, K. Comparative analysis of eddy-current loss in permanent magnet synchronous machine considering PM shape and skew effect using 3-D FEA. *IEEE Trans. Magn.* **2015**, *51*, 1–4. [CrossRef]
15. Yu, Q.; Chu, S.; Li, W.; Tian, L.; Wang, X.; Cheng, Y. Electromagnetic shielding analysis of a canned permanent magnet motor. *IEEE Trans Ind. Electr.* **2020**, *67*, 8123–8130. [CrossRef]
16. Liu, X.; Fu, W.N. A dynamic dual-response-surface methodology for pptimal design of a permanent-magnet motor using finite-element method. *IEEE Trans. Magn.* **2016**, *52*, 1–4.
17. Yu, Q.; Gerling, D. Analytical modeling of a canned switched reluctance machine with multilayer structure. *IEEE Trans. Magn.* **2013**, *49*, 5069–5082. [CrossRef]
18. Fazil, M.; Rajagopal, K.R. Nonlinear dynamic modeling of a single-phase permanent-magnet brushless DC motor using 2-D static finite-element results. *IEEE Trans. Magn.* **2011**, *47*, 781–786. [CrossRef]
19. Yamazaki, K.; Matsumoto, M. 3-D finite element meshing for skewed rotor induction motors. *IEEE Trans. Magn.* **2015**, *51*, 1–4. [CrossRef]
20. Yu, Q.; Wang, X.; Cheng, Y. Magnetic modeling of saliency effect for saturated electrical machines with a new calculation method. *IEEE Trans. Magn.* **2016**, *52*, 1–6. [CrossRef]
21. Uneyama, D.; Akiyama, Y.; Manome, S.; Naruta, T. The proposal of can loss estimation method of a canned motor. In Proceedings of the International Conference on Electronical Machines & Systems, Seoul, Korea, 8–11 October 2007.
22. Liang, Y.P.; Zhang, J.T.; Suo, W.X.; Zhao, B. Eddy current losses analysis of double-cans composite-rotor motor. *Proc. CSEE* **2007**, *29*, 78–83.
23. Dajaku, G.; Gerling, D. Stator slotting effect on the magnetic field distribution of salient pole synchronous permanent-magnet machines. *IEEE Trans. Magn.* **2010**, *46*, 3676–3683. [CrossRef]
24. Yu, Q.; Wang, X.; Cheng, Y.; Tian, L. Analysis of eddy current and loss of a novel canned switched reluctance machine. *IEEE Trans Ind. Electr.* **2018**, *65*, 7640–7647. [CrossRef]